Composites Science and Technology 137 (2016) 69–77

Contents lists available at ScienceDirect

Composites Science and Technology

journal homepage: http://www.elsevier.com/locate/compscitech

# A new theoretical model of the quasistatic single-fiber pullout problem: The energy-based criterion with unloading process

Peng-Yu Pei, Wen-Xue Chang, Hai Qing*, Cun-Fa Gao

*State Key Laboratory of Mechanics and Control of Mechanical Structures, Nanjing University of Aeronautics and Astronautics, Nanjing 210026, China*

ARTICLE INFO

*Article history:*
Received 4 July 2016
Received in revised form
27 September 2016
Accepted 15 October 2016
Available online 30 October 2016

*Keywords:*
Residual thermal stress
Rate-dependence
Potential energy release theory
Unloading process

ABSTRACT

A theoretical analysis for the single-fiber pullout with unload process is presented based on the energy-based debonding criterion and the modified analysis of stress transfer between fiber and matrix(Qing [1]). The relationship between the applied stress and the interfacial relative displacement is expressed as a function of the radial residual thermal stress, fiber pullout rate and volume content as well as the length of reverse frictional sliding. The influence of fiber pullout rate on interfacial frictional coefficient is also taken into consideration. The calculation results show that the applied stress result in further debonding increases with the increase of the radial residual thermal stress and the fiber volume content and the decrease of the fiber pull-out rate. There is a drop for the applied stress when the interface debonding close to the model length and the drops of short models are larger than those of long models. Under different conditions, the model length almost has no influence on the debonding and reverse sliding in unloading processes at the initial debonding region.



## 1. Introduction

It is well known that the efficiency of load transfer across the interface plays a significant role on the mechanical behavior of fiber-reinforced composites [2]. Interfacial debonding and frictional sliding are two main contributors to enhance the toughness of composites. Interfacial strength should be large enough to enable the stress transfer from matrix to fibers. Meanwhile, interfacial strength should be sufficiently low compare with the fiber strength so that the toughness of composite can be enhanced through the interfacial debonding. When debonding occurs, the frictional sliding is the main contributor to the dissipated energy in composite. If the friction is too large, the energy dissipated owing to debonding and pullout will be limited since the debonded region will be small when the fiber breaks. However, if the friction is too small, the pullout work will also be limited even through the debonded region tends to be large.

Several experimental tests, such as single fiber pullout/pushout tests, mircobond, fragmentation and so on, are designed to measure the interfacial properties of composite. Among these test methods, single fiber pullout test has been widely applied to measure both interfacial strength and friction stress. A number of theoretical models have been developed to analyze the stress transfer between the fiber and matrix across the interfaces since first analytic model was developed by Cox [3]. Either a constant friction [4] or Coulomb friction [1,5] is adopted to describe the interfacial frictional sliding in the debonded region. Zhou, Kim and Mai studied the influence of loading method on the stress distributions in the constituents [6]. A few models are developed to analyze the multi-fiber pull-out tests through a three-cylinder model [5,7]. Qing reviewed those basic assumption and limitations of these theoretical models, and developed a new theoretical model in which all relevant stress and strain component have been took into account and all the stress boundary conditions are fulfilled [1]. Recently, Yao et al. investigated the effect of an inhomogeneous interphase on the mechanism of stress transfer [8]. Upadhyaya and Kumar investigated the interphasial/interfacial stress transfer in a three-phase fiber-reinforced composites [9]. Two different criteria to describe the interfacial debonding interfacial strengths are commonly adopted in the models: the interfacial shear strength [10–12] and the potential energy release rate [13–17].

The purpose of the present study is to optimize the application of the single-fiber pullout test in evaluating the interfacial properties. As is pointed out that the interfacial strength and interfacial friction are two main factors to affect the mechanical properties of composites. Normally, these two factors are coupled and have to be

* Corresponding author.
*E-mail addresses:* qinghai@nuaa.edu.cn (H. Qing), cfgao@nuaa.edu.cn (C.-F. Gao).

http://dx.doi.org/10.1016/j.compscitech.2016.10.013
0266-3538/

extracted from the experimental test. Based on the modified analysis of stress [1], a theoretical model is developed to establish the relation between the applied stress and relative displacement during the loading-unloading process. In the unloading process, there is only frictional sliding and no new debonding occurs. That's to say, we can obtain the frictional coefficient through the analysis of unloading process. After we have obtained the frictional properties of interface, we can obtain the interfacial strength, the potential energy release rate of interface in the present study, through analysis the loading process. As a model example the hypothetical glass fiber/epoxy composite is adopted. The influence of radial residual thermal stress, fiber pullout rate, fiber volume contents and model length on applied stress/debonded length and applied stress/relative displacement relationships is investigated.

## 2. Crack-growth and unloading process

A typical mechanical model for single-fiber pullout test is illustrated as shown in Fig. 1. The fiber is located at the centre of a coaxial cylindrical matrix, and the radiuses of fiber and matrix are a and b, respectively. The model length is L, and the length of bonded and debonded region are respective h and l under applied stress$\sigma_p$. In this paper, E and $\upsilon$ are respective young's Modulus and Poison's ratio, and the superscript 'f' and 'm' indicate fiber and matrix, respectively.

### 2.1. Debonding under loading process

The average axial stress of fiber in the bonded region ($0 \le z < h$) can be expressed from Ref. [1] as

$$\overline{\sigma}_z^f = \left(k_1^b \sinh(\lambda z) + k_2^b \cosh(\lambda z) + B_6/B_5\right)\sigma_a \tag{1}$$

In which, $\lambda = \sqrt{2B_5/a}$ , $\sigma_a$ is the applied stress at the end of the fiber, and $B_i$ are listed in Appendix A. The stress boundary conditions of the fiber in the bonded region are

$$\overline{\sigma}_z^f(0) = 0,\ \overline{\sigma}_z^f(h) = \sigma_d \tag{2}$$

Where, $\sigma_d$ is average stress cross the fiber at z = h as shown in Fig. 1. Combining Eqs. (1) and (2), one gets

$$\begin{aligned} k_1^b &= (B_5\sigma_d - B_6\sigma_a + B_6\sigma_a\cosh(\lambda L))/(B_5\sinh(\lambda L))\sigma_a, \\ k_2^b &= -B_6/B_5 \end{aligned} \tag{3}$$

The debonded region is considered as an interfacial crack and its extension is dependent on the energy-based criterion. When potential energy release rate reaches critical $G_{IC}$ which is considered as a material constant, interface debonding occurs and the frictional sliding appears in the debonded region. The debonded region ($h < z \le L$) is presented at the end of fiber as illustrated in Fig. 1(b). The fiber axial stress in the debonded region can be expressed from Ref. [1] as

$$\overline{\sigma}_z^f = k_1^d e^{\lambda_1 z} + k_2^d e^{\lambda_2 z} - \frac{C_9\sigma_a + \sigma_{rs}}{C_8} \tag{4}$$

In which, $\sigma_{rs}$ is the radial residual thermal stress across the interface. $\lambda_{1,2} = \frac{-a \pm \sqrt{a^2 - 16\mu^2 C_7 C_8}}{4\mu C_7}$, $C_i$ are listed in Appendix B, and $\mu$ is the quasi-static frictional coefficient defined from Ref. [18] as

$$\mu = \mu_k + (\mu_s - \mu_k)e^{-(v/C_0)^p} \tag{5}$$

Where, $C_0$ is a constant, $v$ is the pullout speed, $p$ is the damping ratio, $\mu_s$ is the stick-slip frictional coefficient ($v = 0$), and $\mu_k$ is limiting dynamic frictional coefficient ($v \to \infty$). The stress boundary conditions of the fiber in the debonded region are

$$\overline{\sigma}_z^f(h) = \sigma_d,\ \overline{\sigma}_z^f(L) = \sigma_a \tag{6}$$

Combining Eqs. (4) and (6), one gets

$$\begin{aligned} k_1^d &= E_1\sigma_a + E_2\sigma_d + E_3\sigma_{rs} \\ k_2^d &= E_4\sigma_a + E_5\sigma_d + E_6\sigma_{rs} \end{aligned} \tag{7}$$

In which,

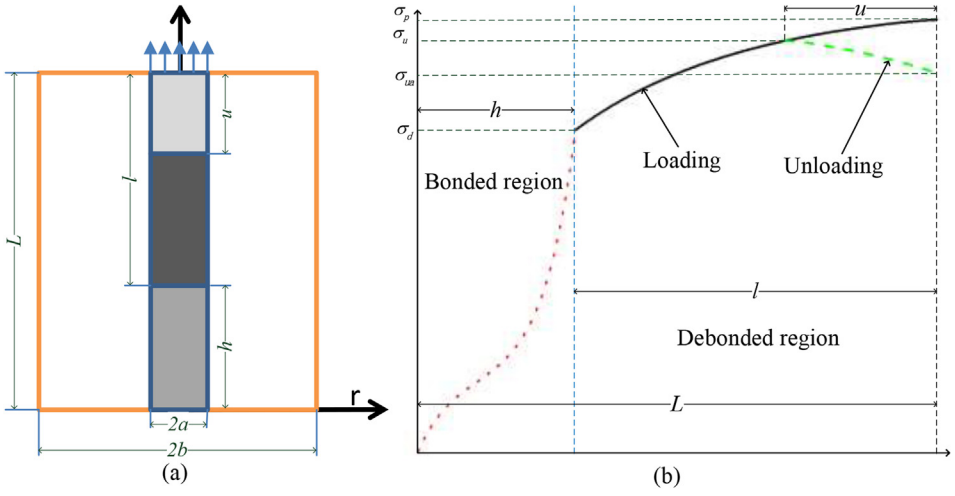


**Fig. 1.** Schematic diagram for single-fiber pullout test: (a) mechanical model and (b) axial stress in fiber.

$$E_1=\frac{(C_8+C_9)e^{h\lambda_2}-C_9e^{L\lambda_2}}{C_8\left(e^{h\lambda_1+L\lambda_2}-e^{h\lambda_2+L\lambda_1}\right)},\quad E_2=\frac{-C_8e^{L\lambda_2}}{C_8\left(e^{h\lambda_1+L\lambda_2}-e^{h\lambda_2+L\lambda_1}\right)},$$
$$E_3=\frac{e^{L\lambda_2}-e^{h\lambda_2}}{C_8\left(e^{h\lambda_1+L\lambda_2}-e^{h\lambda_2+L\lambda_1}\right)},\quad E_4=\frac{C_9e^{L\lambda_1}-(C_8+C_9)e^{h\lambda_1}}{C_8\left(e^{h\lambda_2+L\lambda_1}-e^{h\lambda_1+L\lambda_2}\right)},$$
$$E_5=\frac{C_8e^{L\lambda_1}}{C_8\left(e^{h\lambda_2+L\lambda_1}-e^{h\lambda_1+L\lambda_2}\right)},\quad E_6=\frac{e^{L\lambda_1}-e^{h\lambda_1}}{C_8\left(e^{h\lambda_2+L\lambda_1}-e^{h\lambda_1+L\lambda_2}\right)}$$

An additional condition for debonding is adopted as

$$(\sigma_r|_{r=a}+\sigma_{rs})\big|_{z=L}=0 \tag{8}$$

Where, $\sigma_r|_{r=a}$ is the interfacial radial stress which caused by Poisson contraction, and it can be expressed from Ref. [1] as

$$\sigma_r|_a=C_7\frac{d^2\overline{\sigma}_z^f}{dz^2}+C_8\overline{\sigma}_z^f+C_9\sigma_a \tag{9}$$

Combining Eqs. (8) and (9), one gets the expression of fiber axial stress at $z=h$

$$\sigma_d=\Psi_1(l)\sigma_{rs}+\Psi_2(l)\sigma_a \tag{10}$$

In which,

$$\psi_1=\frac{e^{-L(\lambda_1+\lambda_2)}\left\{C_8e^{L\lambda_1+h\lambda_2}-C_8e^{h\lambda_1+L\lambda_2}-C_7\left[-e^{L\lambda_1+h\lambda_2}\lambda_1^2+e^{h\lambda_1+L\lambda_2}\lambda_2^2+e^{L(\lambda_1+\lambda_2)}\left(\lambda_1^2-\lambda_2^2\right)\right]\right\}}{C_7C_8\left(\lambda_1^2-\lambda_2^2\right)}$$

$$\psi_2=\frac{1}{C_7C_8\left(\lambda_1^2-\lambda_2^2\right)}\Big(e^{-L(\lambda_1+\lambda_2)}\Big(C_8\left(e^{L\lambda_1+h\lambda_2}-e^{h\lambda_1+L\lambda_2}\right)(C_8+C_9)+C_7C_8\left(e^{L\lambda_1+h\lambda_2}\lambda_1^2-e^{h\lambda_1+L\lambda_2}\lambda_2^2\right)-C_7C_9\Big(-e^{L\lambda_1+h\lambda_2}\lambda_1^2+e^{h\lambda_1+L\lambda_2}\lambda_2^2+e^{L(\lambda_1+\lambda_2)}\left(\lambda_1^2-\lambda_2^2\right)\Big)\Big)\Big)$$

From Ref. [1], the normal stresses in fiber and matrix can be expressed as

$$\sigma_z^f=\frac{E^f\left(2\upsilon^fF_2+\left(1-\upsilon^f\right)\varepsilon_{z0}^f\right)}{1-\upsilon^f-2\left(\upsilon^f\right)^2}+\frac{r^2E^f\left(2-\upsilon^f\right)}{2a^2\left(1-\left(\upsilon^f\right)^2\right)}\left(\varepsilon_{za}^f-\varepsilon_{z0}^f\right) \tag{11}$$

$$\sigma_r^f=\frac{E^f\left(F_2+\upsilon^f\varepsilon_{z0}^f\right)}{1-\upsilon^f-2\left(\upsilon^f\right)^2}-\frac{r^2E^f\left(3-4\upsilon^f\right)}{8a^2\left(1-\left(\upsilon^f\right)^2\right)}\left(\varepsilon_{za}^f-\varepsilon_{z0}^f\right) \tag{12}$$

$$\sigma_\theta^f=\sigma_r^f+\frac{r^2E^f}{4a^2\left(1-\left(\upsilon^f\right)^2\right)}\left(\varepsilon_{za}^f-\varepsilon_{z0}^f\right) \tag{13}$$

$$\sigma_z^m=\frac{E^m(2\upsilon^mF_4-(1-\upsilon^m)\varepsilon_{za}^m)}{(1-2\upsilon^m)(1+\upsilon^m)}+\frac{E^m\left(\varepsilon_{zb}^m-\varepsilon_{za}^m\right)\left[2a^2(1-\upsilon^m)^2-r_2\left(2-5\upsilon^m+2(\upsilon^m)^2\right)\right]}{2(1-2\upsilon^m)\left(1-(\upsilon^m)^2\right)\left(2b^2\ln(b/a)-(b^2-a^2)\right)}$$
$$+\frac{E^m\left(\varepsilon_{zb}^m-\varepsilon_{za}^m\right)b^2(-\upsilon^m-4(1-\upsilon^m))^2\log(a)+2\left(2-5\upsilon^m+2(\upsilon^m)^2\right)\log(r)}{2(1-2\upsilon^m)\left(1-(\upsilon^m)^2\right)\left(2b^2\ln(b/a)-(b^2-a^2)\right)} \tag{14}$$

$$\sigma_r^m=\frac{E^m(r^2F_4-(1-2\upsilon^m)F_3)}{r^2(1-2\upsilon^m)(1+\upsilon^m)}+\frac{E^m\left(\varepsilon_{zb}^m-\varepsilon_{za}^m\right)(r^2(3-4\upsilon^m)-4b^2(1-\upsilon^m)\ln(r))}{8\left(1-(\upsilon^m)^2\right)\left(2b^2\ln(b/a)-(b^2-a^2)\right)}$$
$$+\frac{E^m\left(2a^2\varepsilon_{zb}^m\upsilon^m-b^2\left(\varepsilon_{zb}^m-\varepsilon_{za}^m(1-2\upsilon^m)\right)+4b^2\upsilon^m\left(\varepsilon_{za}^m\ln(b)-\varepsilon_{zb}^m\ln(a)\right)\right)}{2\left(1-\upsilon^m-2(\upsilon^m)^2\right)\left(2b^2\ln(b/a)-(b^2-a^2)\right)} \tag{15}$$

$$\sigma_\theta^m=\frac{E^m(r^2F_4+(1-2\upsilon^m)F_3)}{r^2(1-2\upsilon^m)(1+\upsilon^m)}+\frac{E^m\left(\varepsilon_{zb}^m-\varepsilon_{za}^m\right)(r^2(1-4\upsilon^m)-4b^2(1-2\upsilon^m)\ln(r))}{8\left(1-(\upsilon^m)^2\right)\left(2b^2\ln(b/a)-(b^2-a^2)\right)}$$
$$+\frac{E^m\upsilon^m\left(2a^2\varepsilon_{zb}^m(1-\upsilon^m)-b^2\left(\varepsilon_{za}^m(1-2\upsilon^m)+\varepsilon_{zb}^m\right)+4b^2(1-\upsilon^m)\left(\varepsilon_{za}^m\ln(b)-\varepsilon_{zb}^m\ln(a)\right)\right)}{2\left(1-2\upsilon^m-(\upsilon^m)^2+2(\upsilon^m)^3\right)\left(2b^2\ln(b/a)-(b^2-a^2)\right)} \tag{16}$$

In which,

$$\begin{aligned} F_2 &= A_1\sigma_a + A_2\varepsilon_{za}^m + A_3\varepsilon_{za}^f + A_4\varepsilon_{z0}^f \\ F_3 &= A_5\sigma_a + A_6\varepsilon_{za}^m + A_7\varepsilon_{za}^f + A_8\varepsilon_{z0}^f \\ F_4 &= A_9\sigma_a + A_{10}\varepsilon_{za}^m + A_{11}\varepsilon_{za}^f + A_{12}\varepsilon_{z0}^f \end{aligned} \tag{17}$$

$A_i$ are listed in Appendix C.

In the bonded region,

$$\varepsilon_{za}^f = B_3\overline{\sigma}_z^f + B_4\sigma_a \tag{18}$$

$$\varepsilon_{z0}^f = B_3\varepsilon_{za}^f + B_2\sigma_a \tag{19}$$

$$\varepsilon_{za}^m = \varepsilon_{za}^f = B_3\overline{\sigma}_z^f + B_4\sigma_a \tag{20}$$

In the debonded region,

$$\varepsilon_{za}^f = \frac{a^2\left(1+\upsilon^f\right)}{2(C_6-1)\mathrm{E}^f}\frac{\mathrm{d}^2\overline{\sigma}_z^f}{\mathrm{d}z^2} + \frac{C_5}{1-C_6}\overline{\sigma}_z^f + \frac{C_4}{1-C_6}\sigma_a \tag{21}$$

$$\varepsilon_{z0}^f = C_4\sigma_a + C_5\overline{\sigma}_z^f + C_6\varepsilon_{za}^f \tag{22}$$

$$\varepsilon_{za}^m = C_1\sigma_a + C_2\varepsilon_{z0}^f + C_3\varepsilon_{za}^f \tag{23}$$

The shear stresses in fiber and matrix can be expressed from Ref. [1] as

$$\tau_{rz}^f = r\tau_i/a \tag{24}$$

$$\tau_{rz}^m = \frac{a\tau_i}{b^2-a^2}\left(\frac{b^2}{r} - r\right) \tag{25}$$

In which, $\tau_i$ is interfacial shear stress and can be expressed from Ref. [1] as

$$\tau_i = -\frac{a}{2}\frac{d\overline{\sigma}_z^f}{dz} \tag{26}$$

The debonding appears when the following equation is satisfied

$$G_{IC} = \frac{\partial U_t}{\partial(2\pi a l)} \tag{27}$$

In which, $U_t$ is the total elastic strain energy of model and can be calculated as

$$\begin{aligned} U_t = {} & \frac{\pi}{2}\int_0^h\int_0^a\left(\sigma_r^f\varepsilon_r^f + \sigma_z^f\varepsilon_z^f + \sigma_\theta^f\varepsilon_\theta^f + \tau_{rz}^f\gamma_{rz}^f\right)rdrdz + \frac{\pi}{2}\int_0^h\int_a^b(\sigma_r^m\varepsilon_r^m \\ & + \sigma_z^m\varepsilon_z^m + \sigma_\theta^m\varepsilon_\theta^m + \tau_{rz}^m\gamma_{rz}^m)rdrdz + \frac{\pi}{2}\int_h^L\int_0^a\left(\sigma_r^f\varepsilon_r^f + \sigma_z^f\varepsilon_z^f\right. \\ & \left. + \sigma_\theta^f\varepsilon_\theta^f + \tau_{rz}^f\gamma_{rz}^f\right)rdrdz + \frac{\pi}{2}\int_h^L\int_a^b(\sigma_r^m\varepsilon_r^m + \sigma_z^m\varepsilon_z^m + \sigma_\theta^m\varepsilon_\theta^m \\ & + \tau_{rz}^m\gamma_{rz}^m)rdrdz \end{aligned} \tag{28}$$

Combining Eqs. (27) and (28), one can express $\sigma_d$ as a function of $l$, $\sigma_a$, dimension of model and so on.

### 2.2. Frictional sliding in unloading process

When the applied stress increases to $\sigma_p$, the interfacial debonding extends to $l$ ($0 < l \le L$). The interfacial frictional stress is

$$\tau_i = \mu(\sigma_r|_a + \sigma_{rs}) \tag{29}$$

When we reduces applied stress from the corresponding$\sigma_p$ to $\sigma_{ua}$ gradually, the reduction of applied stress causes the reverse frictional sliding of interface, and the length of reverse sliding region is assumed to be u as shown in Fig. 1. The interfacial friction in the reverse sliding region during the unloading process is expressed as

$$\tau_i = -\mu(\sigma_r|_a + \sigma_{rs}) \tag{30}$$

Combining Eqs. (9), (26) and (30), one can obtain

$$\frac{d^2\overline{\sigma}_z^f}{dz^2} - \frac{a}{2\mu C_7}\frac{d\overline{\sigma}_z^f}{dz} + \frac{C_8}{C_7}\overline{\sigma}_z^f + \frac{C_9\sigma_{ua}+\sigma_{rs}}{C_7} = 0 \tag{31}$$

A general solution of ordinary differential Eq. (31) is

$$\overline{\sigma}_z^f = k_1^u e^{\lambda_3 z} + k_2^u e^{\lambda_4 z} - \frac{C_9\sigma_{ua}+\sigma_{rs}}{C_8} \tag{32}$$

Where, $\lambda_{3,4}$ are

$$\lambda_{3,4} = \frac{a \pm \sqrt{a^2 - 16\mu^2 C_7 C_8}}{4\mu C_7}$$

The stress boundary conditions for Eq. (32) are

$$\overline{\sigma}_z^f(L) = \sigma_{ua}, \quad \overline{\sigma}_z^f(L-u) = \sigma_u \tag{33}$$

Combining Eqs. (32) and (33), one gets

$$k_1^u = \frac{\left(C_9(1-e^{-u\lambda_4}) - C_8e^{-u\lambda_4}\right)\sigma_{ua} + C_8\sigma_u + (1-e^{-u\lambda_4})\sigma_{rs}}{C_8\left(e^{(L-u)\lambda_3} - e^{L\lambda_3 - u\lambda_4}\right)}$$

$$k_2^u = \frac{\left(C_9\left(1-e^{-u\lambda_3}\right) - C_8e^{-u\lambda_3}\right)\sigma_{ua} + C_8\sigma_u + \left(1-e^{-u\lambda_3}\right)\sigma_{rs}}{C_8\left(e^{(L-u)\lambda_4} - e^{-u\lambda_3 + L\lambda_4}\right)}$$

During the unloading process, the frictional interfacial stress at $z = L-u$ switches the direction, which requires $\tau(L-u)$=0, e.g.,

$$\sigma_r|_a + \sigma_{rs} = 0 \tag{34}$$

Meanwhile, during the unloading process, the axial stress distribution of fiber in the region of $l < z \le L-u$ is exact similar to that under the applied loading$\sigma_p$. Therefore,

$$k_1^d e^{\lambda_1(L-u)} + k_2^d e^{\lambda_2(L-u)} - \frac{C_9\sigma_p+\sigma_{rs}}{C_8} = \sigma_u \tag{35}$$

Substituting Eq. (35) into (32) and combining it with Eq. (34), one can express the unloading stress as a function of reverse sliding region u as

$$\begin{aligned} \sigma_{ua} = {} & ((C_7(-1+e^{u\lambda_4})\lambda_3^2 - C_7(-1+e^{u\lambda_3})\lambda_4^2 - C_8(e^{u\lambda_3} \\ & - e^{u\lambda_4}))\sigma_{rs} + (C_7C_8e^{u\lambda_4}\lambda_3^2 - C_7C_8e^{u\lambda_3}\lambda_4^2 - C_8^2(e^{u\lambda_3} \\ & - e^{u\lambda_4}))\sigma_u)/(-C_7C_9((-1+e^{u\lambda_4})\lambda_3^2 - (-1+e^{u\lambda_3})\lambda_4^2) \\ & + C_8(C_9(e^{u\lambda_3} - e^{u\lambda_4}) + C_7(\lambda_3^2 - \lambda_4^2))\Big) \end{aligned} \tag{36}$$

For a single-fiber pullout test, it's easy to measure the applied stress and the related displacement between fiber and matrix. We have expressed the applied stresses $\sigma_a$ and $\sigma_{ua}$ above. The total related displacement$\delta$ at interface is contributed from two regions: sliding region $\delta_d$ $(h<z<L-u)$ and reverse sliding region $\delta_u(L-u<z<L)$, e,g., $\delta$=$\delta_d+\delta_u$. $\delta_d$ can be calculated from

$$\delta_d = \int_h^{L-u} \left(\varepsilon_{za}^f - \varepsilon_{za}^m\right) dz \tag{37}$$

Where, $\varepsilon_{za}^f$ and $\varepsilon_{za}^m$ are respectively defined in Eqs. (21) and (23) under the maximum applied stress $\sigma_p$. In reverse sliding region, according to Eqs. (21) and (23), the strain components in fiber and matrix can be expresses as

$$\varepsilon_{zua}^f = \frac{a^2\left(1+\upsilon^f\right)}{2(C_6-1)E^f}\frac{d^2\overline{\sigma}_z^f}{dz^2} + \frac{C_5}{1-C_6}\overline{\sigma}_z^f + \frac{C_4}{1-C_6}\sigma_{ua} \tag{38}$$

$$\varepsilon_{zu0}^f = C_4\sigma_{ua} + C_5\overline{\sigma}_z^f + C_6\varepsilon_{zua}^f \tag{39}$$

$$\varepsilon_{zua}^m = C_1\sigma_{ua} + C_2\varepsilon_{zu0}^f + C_3\varepsilon_{zua}^f \tag{40}$$

Where, $\varepsilon_{zua}^f$ and $\varepsilon_{zu0}^f$ are respective axial strains of fiber at $r=a$ and $r=0$, while $\varepsilon_{zua}^m$ is the axial strain of matrix at $r=a$. Therefore, the relative displacement in the reverse sliding region $\delta_u$ can be calculated from the following equation

$$\delta_u = \int_{L-u}^{L} \left(\varepsilon_{zua}^f - \varepsilon_{zua}^m\right) dz \tag{41}$$

## 3. Numerical evaluation results and discussion

Several numerical examples are illustrated the important results of present model for a hypothetical glass/epoxy composite. The elastic properties of the fiber and matrix are given from Ref. [19] by:$E^f=72GPa$,$\upsilon^f=0.26$,$E^m=3.79$ GP$a$ and $\upsilon^m=0.37$. The radius of fiber is fixed to be 0.1 mm, and the critical energy release rate $G_{IC}$ of the interface is 0.1 J/m$^2$. The constants to define the frictional coefficient from Ref. [18] are$p=5$,$C_0=10$ mm/min, $\mu_s=1.5$ and $\mu_k=1.25$(in Eq. (5)).

Fig. 2 shows the relationship of the applied stress $\sigma_a$ result in further debonding with debonding length h for$\sigma_{rs}=10$ MPa and $v=10$ mm/$min$ based three different models to calculate the elastic strain energy. The model of Hsueh only took into account the axial deformation mechanism to calculate the elastic strain energy [14]. That's to say,

$$U_t = \pi\int_0^L\int_0^a \sigma_z^f\varepsilon_z^f r dr dz + \pi\int_0^L\int_a^b \sigma_z^m\varepsilon_z^m r dr dz \tag{42}$$

The model of Zhou et al. also took into account the shear deformation in matrix besides the axial deformation to calculate the strain energy [15].

$$U_t = \pi\int_0^L\int_0^a \sigma_z^f\varepsilon_z^f r dr dz + \pi\int_0^L\int_a^b (\sigma_z^m\varepsilon_z^m + \tau_{rz}^m\gamma_{rz}^m) r dr dz \tag{43}$$

Present model takes into account all the deformation mechanism according to Eq. (28). One can see from Fig. 2 that the applied stresses to cause the further debonding with the debonding length show a same trend: the applied stress to cause further debonding increases to a maximal value and then decreases till the fully debonding with the increase of the debonding length. The applied stress to cause the further debonding is distinctly influenced by the methods to calculate the elastic strain energy because the models of Zhou et al. and Hsueh et al. oversimplifies the deformation mechanism. The predicted result from present model is higher than those from other two models in the initial debonding region, while is higher than that from Zhou et al. while lower than that from Hsueh et al. in the last debonding region.

Distributions of the applied stress result in further debonding with the debonding length are plotted in Figs. 3–5 for different radial residual thermal stresses, fiber pullout rates, fiber volume contents and model lengths. It can be seen from Figs. 3–5 that under different conditions, the applied stress result in further debonding increases with the increase of the debonded length to some extent and then decreases till the fully debonding. Furthermore, there is almost no difference for the relationship between the applied stress and the debonded length in the initial debonding region. A drop for applied stress is observed when the debonding

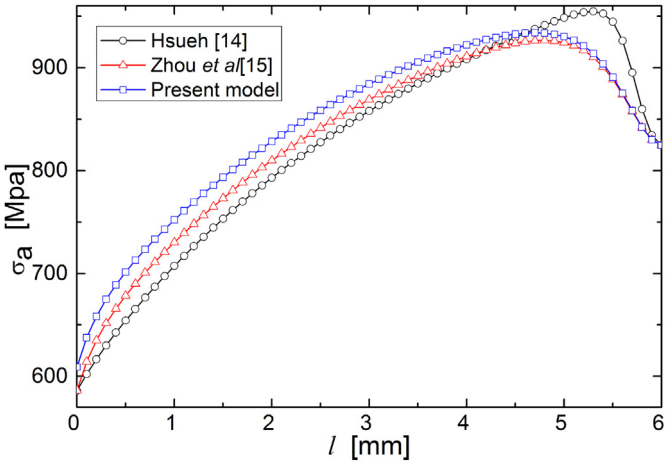


**Fig. 2.** Variation of the applied stress with the debonded length for $b=10a$, $v$=0 mm/min, $\sigma_{rs}=10$ MPa and $L=6b$.

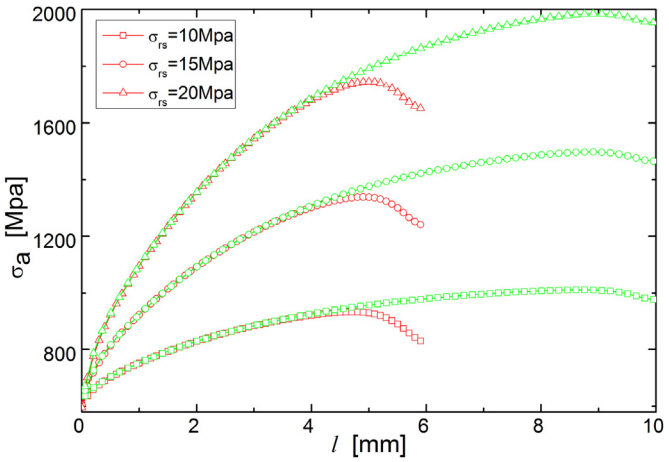


**Fig. 3.** The influence of thermal residual stress on the applied stress to cause further debonding for $b=10a$ and $v$=0mm/min.

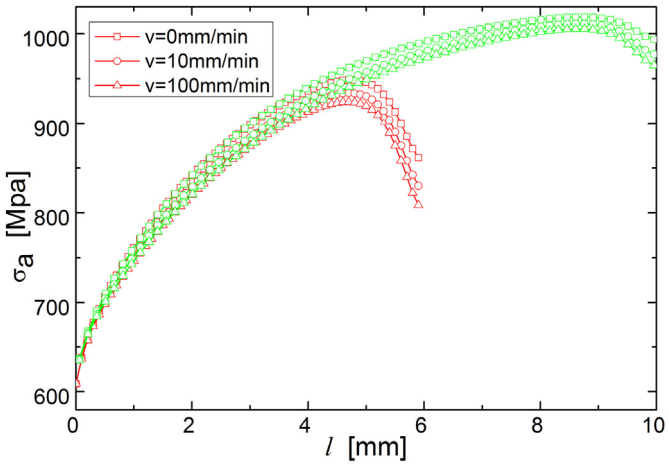


**Fig. 4.** The influence of fiber pullout rate on the applied stress to cause further debonding for $b = 10a$ and $\sigma_{rs}$=10 MPa.

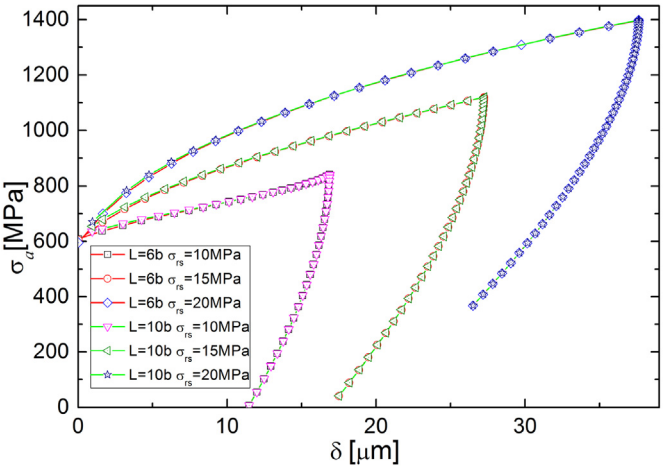


**Fig. 6.** The influence of thermal residual stress on the relative displacement of fiber and matrix for $b = 10a$ and $v = 10$mm/*min*.

close to model end, and the drop decreases with the increase of the model length. It can be seen from Fig. 3 that the initial debonding stress is independent on the radial residual thermal stress and the applied stress result in further debonding is an increasing function of the radial residual thermal stress. From Fig. 4, one can see that the applied stress result in further debonding is a decreasing function of the fiber pullout rate since the frictional coefficient is a decreasing function of the pullout rate. However, the influence of fiber pullout rate on the applied stress result in further debonding is not so significant since the frictional coefficient changes a little(According to Eq. (5), the frictional coefficients are 1.5, 1.342 and 1.25 corresponding to 0 mm/min, 10 mm/min and 100 mm/min, respectively). Fig. 5 shows that the influence of the fiber volume content on the applied stress result in further debonding is significant and the applied stress result in further debonding is an increasing function with the fiber volume content.

The influence of the radial residual thermal stresses, fiber pullout rates, fiber volume contents and model lengths on the applied stress result in further debonding is investigated above. It has been mentioned previously that there are mainly two interfacial properties, interfacial strength and frictional coefficient, for interface to dominate the properties of composite. With the increase of the applied stress, new debonding occurs and frictional sliding in the debonded region occurs, so that it's not easy to evaluate both the interfacial strength and frictional coefficient during the debonding process. However, during the unloading process, there is only frictional sliding in the debonded region without new debonding, thus one can easily determine the frictional coefficient in the unloading process.

Fig. 6 shows the influence of the radial residual thermal stress on relationship of applied stress $\sigma_a$ versus relative displacement $\delta$ for $b = 10a$ and $v = 10$ mm/*min* with different model lengths, in which the radial residual thermal stresses change from 10 MPa, 15 MPa–20 MPa, respectively. When the debonded length is small related to the model length(for example $l = 2.2b$ here), it's hardly to distinguish the influence of the model length for either loading and unloading processes. The results agree well with the results from Fig. 3 for loading process. Meanwhile, the relative displacement at $u = l$ increases with the increase of the radial residual thermal stress under same debonding length. The unloading process stops when the reverse sliding region $u$ equals to the debonded length $l$. The unloading stress and relative displacement at $u = l$ increase with the increase of radial residual thermal stress.

Fig. 7 shows the influence of fiber pullout rate on the relationship of applied stress $\sigma_a$ versus relative displacement $\delta$ for $b = 10a$

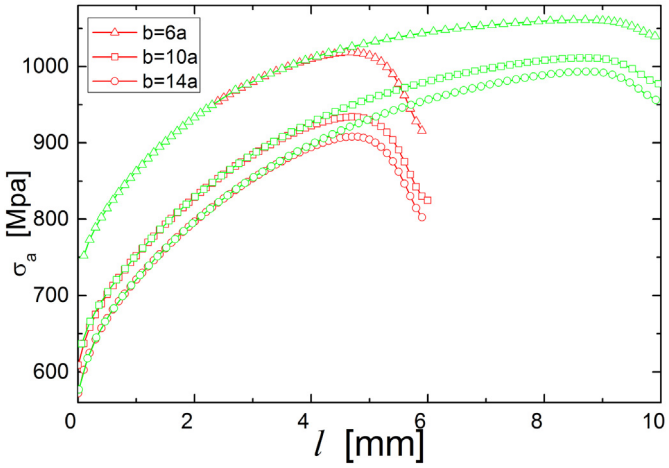


**Fig. 5.** The influence of fiber volume content on the applied stress to cause further debonding for $v = 10$ mm/*min* and $\sigma_{rs} = 10$MPa.

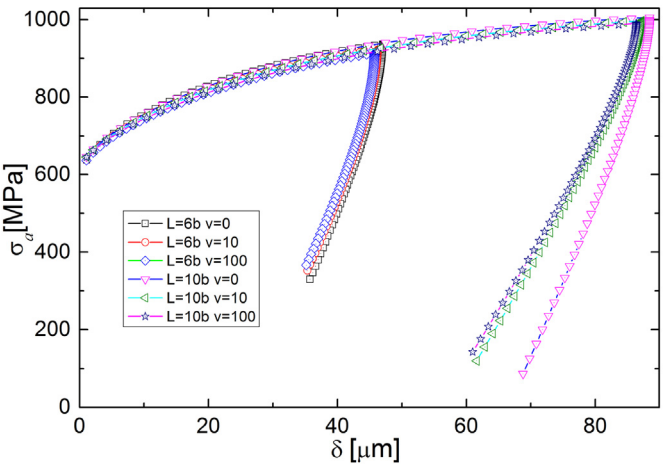


**Fig. 7.** The influence of fiber pullout rate on the relative displacement of fiber and matrix for and $b = 10a$ and.$\sigma_{rs} = 10$ MPa.

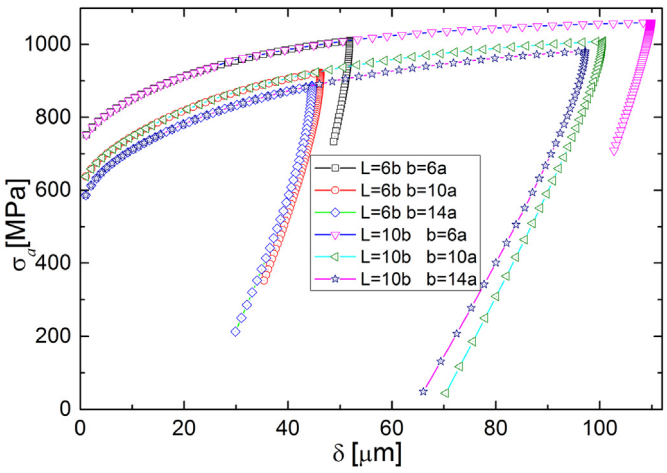


**Fig. 8.** The influence of fiber volume content on the relative displacement of fiber and matrix for $\sigma_{rs} = 10$ MPa and $v = 0$mm/*min*.

and $\sigma_{rs} = 10$ MPa with different model lengths, in which fiber pullout rate changes from 0 mm/min, 10 mm/min to 100 mm/min, respectively. The unloading process starts when $l = 4b$ for $L = 6b$ and $l = 7b$ for $L = 10b$, respectively. The difference of the applied stress $\sigma_a$ versus relative displacement $\delta$ is not significant in the initial debonding region, which agrees well with the results from Fig. 4. With the increase of fiber pullout rate, the unloading stresses at $u = l$ increases while the relative displacements at $u$=$l$ decreases.

Fig. 8 shows the influence of fiber volume content on the relationship of applied stress $\sigma_a$ versus relative displacement $\delta$ for $\sigma_{rs} = 10$MPa and $v = 0$ mm/*min* with different model lengths, in which the fiber volume contents are given as b = 6a, b = 10a and b = 14a, respectively. The unloading process starts when $l = 4b$ for $L = 6b$ and $l = 7b$ for$L = 10b$, respectively. The difference of the applied stress $\sigma_a$ versus relative displacement $\delta$ is not significant in the initial debonding region, which agrees well with the results from Fig. 5. Both the unloading stresses and the relative displacements at $u = l$ increase with the increase of fiber volume contents.

## 4. Conclusions

A theoretical model is developed to establish the relationship between the applied stress and relative displacement during the loading-unloading process based on the debonding criterion of energy release rate and the modified analysis of stress (Qing, 2013). The influence of radial residual thermal stress, fiber pullout rate, fiber volume contents and model length on loading and unloading processes is investigated through the theoretical model. The study results show that both normal deformation along the radial and circumferential directions as well as shear deformation should be taken into account to calculate the elastic strain energy for single fiber pullout model. The model length almost has no influence on the debonding and unloading processes at the initial debonding region under different conditions of radial residual thermal stress, fiber pullout rate and fiber volume contents. There is a drop for applied stress when the debonding close to model end, and the drop decreases with the increase of the model length. When the unloading stops($u = l$), the unloading stress increases with the increase of radial residual thermal stress, fiber pullout rate and fiber volume content.

## Acknowledge

The work was supported by Natural Science Foundation of Jiangsu Province of China (BK20140802), the Fundamental Research Funds for the Central Universities (No. NE2014401), the Research Fund of State Key Laboratory of Mechanics and Control of Mechanical Structures (Nanjing University of Aeronautics and Astronautics) (Grant No. MCMS-0214K01 and MCMS-0216G01), the Priority Academic Program Development of Jiangsu Higher Education Institutions and the Scientific Research Foundation for the Returned Overseas Chinese Scholars, State Education Ministry.

## Appendix A. Coefficients for bonded region

$$B_1 = \left(a\left(A_2 + A_3 - A_{10} - A_{11} - 1/8\left(1 - \upsilon^f\right)\right) - (A_6 + A_7)/a - \frac{E^f(1+\upsilon^m)(a^3/8 - ab^2\ln(a)/2)}{(b^2 - a^2)E^m(1+\upsilon^f)(1-\upsilon^m)}\right)B_0$$

$$B_2 = (a(A_1 - A_9) - A_5/a)B_0$$

$$B_3 = \frac{8\left(1-\upsilon^f\right)\left(1-\upsilon^f - 2\left(\upsilon^f\right)^2\right)}{E^f(2 + 2B_1 + \upsilon^f(8A_2 + 8A_3 - 3B_1 - 5 + 8A_4B_1 + (2 - 8A_2 - 8A_3 + 2B_1 - 8A_4B_1)\upsilon^f)}$$

$$B_4 = -\frac{2B_2 + \upsilon^f(8A_1 - 3B_2 + 8A_4B_2 + (2B_2 - 8A_1 - 8A_4B_2)\upsilon^f)}{2 + 2B_1 + \upsilon^f(8A_2 + 8A_3 - 3B_1 - 5 + 8A_4B_1 + (2 - 8A_2 - 8A_3 + 2B_1 - 8A_4B_1)\upsilon^f}$$

$$B_5 = \frac{E^f(B_1 - 1)B_3}{a(1+\upsilon^f)}$$

$$B_6 = \frac{E^f((1 - B_1)B_4 - B_2)}{a(1+\upsilon^f)}$$

Where,

$$B_0 = 1/\left[a(A_{12} - A_4) + A_8/a - a/8(1-\upsilon^f) - \frac{E^f(1+\upsilon^m)(a^3/8 - ab^2\ln(a)/2)}{(b^2-a^2)E^m(1+\upsilon^f)(1-\upsilon^m)}\right]$$

## Appendix B. Coefficients for debonded region

$$C_1 = \frac{a^2(A_1 - A_9) - A_5}{a^2(A_{10} - A_2) + A_6}$$

$$C_2 = \frac{a^2(A_3 - A_{11} - 1/8\left(1 - \upsilon^f\right) + \frac{aE^f(a^3 - 4ab^2\ \log(a))(1+\upsilon^m)}{8E^m(b^2-a^2)(1+\upsilon^f)(1-\upsilon^m)} - A_7}{a^2(A_{10} - A_2) + A_6}$$

$$C_3 = \frac{a^2(A_4 - A_{12} - 1/8\left(1 - \upsilon^f\right) - \frac{aE^f(a^3 - 4ab^2\ \log(a))(1+\upsilon^m)}{8E^m(b^2-a^2)(1+\upsilon^f)(1-\upsilon^m)} - A_8}{a^2(A_{10} - A_2) + A_6}$$

$$C_4 = -\frac{8(A_1 + A_2C_1)\left(1 - \upsilon^f\right)\upsilon^f}{2 + \upsilon^f(8A_3 + 8A_2C_2 - 3 + (2 - 8A_3 - 8A_2C_2)\upsilon^f)}$$

$$C_5 = \frac{8\left(1 - \upsilon^f\right)\left(1 + \upsilon^f\right)\left(1 - 2\upsilon^f\right)}{E^f(2 + \upsilon^f(8A_3 + 8A_2C_2 - 3 + (2 - 8A_3 - 8A_2C_2)\upsilon^f))}$$

$$C_6 = -\frac{2 + \upsilon^f\left(8A_4 + 8A_2C_3 - 5 + (2 - 8A_4 - 8A_2C_3)\upsilon^f\right)}{2 + \upsilon^f(8A_3 + 8A_2C_2 - 3 + (2 - 8A_3 - 8A_2C_2)\upsilon^f)}$$

$$A_3 = \frac{1 - 2\upsilon^f}{8a^2\left(b^2 - a^2\right)\left(1 - \upsilon^f\right)\left(\upsilon^f - \upsilon^m\right)}\Big[-a^2(b^2 - a^2)(2 + 3\upsilon^m + \upsilon^f(3 - 2\upsilon^m)) + 2\left(1 - \upsilon^f\right)(a^4 - 4a^2b^2 + 3b^4 - 4b^4\ln(b/a) + (2b^4 - 2a^2b^2 - 4b^4\ln(b/a))\upsilon^m)\Big]$$

$$A_4 = -\frac{1}{8a^2(b^2 - a^2)\left(1 - \upsilon^f\right)\left(\upsilon^f - \upsilon^m\right)}\Big[a^2\left(b^2 - a^2\right)(2 + 2\left(\upsilon^f\right)^2 - 3\upsilon^m - \upsilon^f(3 - 2\upsilon^m)) + 2\left(1 - 3\upsilon^f + 2\left(\upsilon^f\right)^2\right)(a^4 - 4a^2b^2 + 3b^4 - 4b^4\ln(b/a) + (2b^4 - 2a^2b^2 - 4b^4\ln(b/a))\upsilon^m)\Big]$$

$$A_5 = -\frac{a^2b^2(1 + \upsilon^m)}{(b^2 - a^2)E^m\left(\upsilon^f - \upsilon^m\right)}$$

$$A_6 = \frac{b^2(1 + \upsilon^m)}{2\left(\upsilon^f - \upsilon^m\right)}$$

$$A_7 = b^2A_0\Big[-4a^4 + 10a^2b^2 - 6b^4 + 8b^4\ln(b/a) + \left(a^4 - 3a^2b^2 + 2b^4 - 4a^2b^2\ln(\mathrm{b/a})\right)\upsilon^m + 4\left(b^2 - a^2\right)\left(b^2 - a^2 - 2b^2\ln(b/a)\right)(\upsilon^m)^2 + a^2\upsilon^f\left(b^2 - a^2 + 4b^2\ln(b/a)(1 - 2\upsilon^m)\right)\Big]$$

$$C_7 = \frac{a^2(3 - 3C_3 - 8A_3C_6 - 8(A_4 + A_2(C_3 + C_2C_6))(1 - \upsilon^f) + 2\upsilon^f(C_6 + 4A_3C_6 + 4\upsilon^f - 5)\Big)}{16(1 - C_6)(1 - 3\upsilon^f + 2\left(\upsilon^f\right)^2\Big)}$$

$$A_8 = b^2A_0\Big[6b^4 - 6a^2b^2 - 8b^4\ln(b/a) + a^2\upsilon^f(3b^2 - 3a^2 - 4b^2\ln(b/a) - 4(b^2 - a^2 - 2b^2\ln(b/a))\upsilon^m - (2b^4 - 3a^4 + a^2b^2 - 4a^2b^2\ln(\mathrm{b/a}))\upsilon^m + 4\left(b^2 - a^2\right)(a^2 - b^2 + 2b^2\ln(b/a))(\upsilon^m)^2\Big]$$

$$C_8 = \frac{C_5E^f(A_3 + A_4 + A_2C_2 + A_2C_3 + \upsilon^f\Big)}{\Big(1 - C_6)(1 - \upsilon^f - 2\left(\upsilon^f\right)^2\Big)}$$

$$C_9 = \frac{E^f(A_1(1 - C_6) + A_2(C_1 + (C_2 + C_3)C_4 - C_1C_6) + C_4(A_3 + A_4 + \upsilon^f))}{\Big(1 - C_6)(1 - \upsilon^f - 2\left(\upsilon^f\right)^2\Big)}$$

## Appendix C. Coefficients related to elastic properties and geometrical parameters

$$A_1 = \frac{1 - \upsilon^f - 2\left(\upsilon^f\right)^2}{E^f\left(\upsilon^f - \upsilon^m\right)}$$

$$A_2 = \frac{E^m(b^2 - a^2)(1 - \upsilon^f - 2\left(\upsilon^f\right)^2\Big)}{2a^2E^f\left(\upsilon^f - \upsilon^m\right)}$$

$$A_9 = -\frac{a^2(1 - \upsilon^m - 2(\upsilon^m)^2\Big)}{(b^2 - a^2)E^m(\upsilon^f - \upsilon^m)}$$

$$A_{10} = \frac{1 - \left(1 + \upsilon^f\right)\upsilon^m}{2\left(\upsilon^f - \upsilon^m\right)}$$

$$A_{11} = A_0\Big[10a^2b^2 - 6b^4 - 4a^4 + 8b^4\ln(b/a) + \Big(b^4 - a^4 - 4a^2b^2\ln a + 4b^4\ln b\Big)v^f - v^m((9a^4 - 22a^2b^2 + 13b^4 + 4b^2\Big(a^2 + b^2\Big)\ln a - 20b^4\ln b + (10a^4 + 6b^4 - 16a^2b^2 - 16b^4\ln(b/a))v^f) - (v^m)^2\Big(6\Big(a^2 - b^2\Big)^2 - 8b^4\ln(b/a) + 8(\Big(a^2 - b^2\Big)^2 - b^4\ln(b/a))v^f)\Big)\Big]$$

$$A_{12} = A_0\Big[6b^4 - 6a^2b^2 - 8b^4\ln(b/a) - \Big(b^4 + 3a^4 - 4a^2b^2 - 4a^2b^2\ln a + 4b^4\ln b\Big)v^f + v^m\Big(\Big(3a^4 + 10a^2b^2 - 13b^4 - 4b^2\Big(a^2 + 4b^2\Big)\ln a + 20b^4\ln b + 2\Big(a^4 - 3b^4 + 2a^2b^2 + 8b^4\ln(b/a)\Big)v^f\Big) - (v^m)^2\Big(2a^4 + 4a^2b^2 - 6b^4 + 8b^4\ln(b/a) + 8b^2\Big(a^2 - b^2 + 2b^2\ln(b/a)\Big)v^f\Big)\Big)\Big]$$

Where, $A_0 = \frac{E^f(1+v^m)}{8(b^2-a^2)^2E^m(1+v^f)(1-v^m)(v^f-v^m)}$.

## References


[1] H. Qing, A new theoretical model of the quasistatic single-fiber pullout problem: analysis of stress field, Mech. Mater. 60 (1) (2013) 66–79.
[2] J.K. Kim, Y.W. Mai, Engineered Interfaces in Fiber Reinforced Composites, Elsevier, Oxford, 1998.
[3] H.L. Cox, The elasticity and strength of paper and other fibrous materials, Br. J. Appl. Phys. 3 (3) (1952) 72–79.
[4] S.Y. Fu, B.L. Zhou, X. Chen, C.F. Xu, G.H. He, C.W. Lung, Some further considerations of the theory of fiber debonding and pull-out from an elastic matrix 1. Constant interfacial frictional shear-stress, Composites 24 (1) (1993) 5–11.
[5] J.W. Hutchinson, H.N. Jensen, Model of fiber debonding and pullout in brittle composites with friction, Mech. Mater. 9 (2) (1990) 139–163.
[6] L.M. Zhou, J.K. Kim, Y.W. Mai, On the single fibre pull-out problem: effect of loading method, Compos. Sci. Technol. 45 (2) (1992) 153–160.
[7] S.Y. Fu, C.Y. Yue, X. Hu, Y.W. Mai, Analyses of the micromechanics of stress transfer in single- and multi-fiber pull-out tests, Compos. Sci. Technol. 60 (4) (2000) 569–579.
[8] Y. Yao, S.H. Chen, P.J. Chen, The effect of a graded interphase on the mechanism of stress transfer in a fiber-reinforced composite, Mech. Mater. 58 (3) (2013) 35–54.
[9] P. Upadhyaya, S. Kumar, Micromechanics of stress transfer through the interphase in fiber-reinforced composites, Mech. Mater. 89 (2015) 190–201.
[10] C.H. Hsueh, Interfacial debonding and fiber pullout stresses of fiber-reinforced composites VII improved analyses for bonded interfaces, Mater. Sci. Eng. A 154 (2) (1992) 125–132.
[11] H.Y. Liu, X. Zhang, Y.W. Mai, X.X. Dao, On steady-state fiber pullout II computer simulation, Compos. Sci. Technol. 59 (19) (1999) 2191–2199.
[12] W.X. Chang, H. Qing, C.F. Gao, A new theoretical model of the quasistatic single-fiber pullout problem: a rate-dependent interfacial bond strength, Mech. Mater. 94 (2016) 132–141.
[13] Y.C. Gao, Y.W. Mai, B. Cotterell, Fracture of fiber-reinforced materials, Z. Angew. Math. Phys. Zamp 39 (4) (1988) 550–572.
[14] C.H. Hsueh, Interfacial debonding and fiber pullout stresses of fiber-reinforced composites VIII: the energy-based debonding criterion, Mater. Sci. Eng. A 159 (1) (1992) 65–72.
[15] L.M. Zhou, J.K. Kim, Y.W. Mai, Interfacial debonding and fiber pullout stresses Part II a new model based on the fracture mechanics approach, J. Mater. Sci. 27 (12) (1992) 3155–3166.
[16] Y.S. Chai, B.S. Choi, K.J. Yang, Improved modeling of the effects of thermal residual stresses on single fiber pull-out problem, J. Mech. Sci. Technol. 15 (7) (2001) 823–830.
[17] Q.H. Meng, Z.Q. Wang, Theoretical analysis of interfacial debonding and fiber pull-out in fiber-reinforced polymer-matrix composites, Arch. Appl. Mech. 85 (6) (2015) 745–759.
[18] G.L. Povirk, A. Needleman, Finite element simulation of fiber pullout, J. Eng. Mater. Technol. 115 (3) (1993) 286–291.
[19] H. Qing, L. Mishnaevsky, Unidirectional high fiber content composites: automatic 3D FE model generation and damage simulation, Comput. Mater. Sci. 47 (2) (2009) 548–555.